Model of Creation and Evolution of Stable Electropores for DNA Delivery

Kyle C. Smith,* John C. Neu,*† and Wanda Krassowska*
*Department of Biomedical Engineering, Duke University, Durham, North Carolina 27708; and †Department of Mathematics, University of California, Berkeley, California 94720

ABSTRACT Electroporation, in which electric pulses create transient pores in the cell membrane, is becoming an important technique for gene therapy. To enable entry of supercoiled DNA into cells, the pores should have sufficiently large radii (>10 nm), remain open long enough for the DNA chain to enter the cell (milliseconds), and should not cause membrane rupture. This study presents a model that can predict such macropores. The distinctive features of this model are the coupling of individual pores through membrane tension and the electrical force on the pores, which is applicable to pores of any size. The model is used to explore the process of pore creation and evolution and to determine the number and size of pores as a function of the pulse magnitude and duration. Next, our electroporation model is combined with a heuristic model of DNA uptake and used to predict the dependence of DNA uptake on pulsing parameters. Finally, the model is used to examine the mechanism of a two-pulse protocol, which was proposed specifically for gene delivery. The comparison between experimental results and the model suggests that this model is well-suited for the investigation of electroporation-mediated DNA delivery.

INTRODUCTION

Electroporation, a technique in which electric pulses are used to create transient pores in the cell membrane, is used for the delivery of biologically active molecules into cells (Dev et al., 2000; Potter, 1988; Weaver and Chizmadzhev, 1996). An emerging application of electroporation is gene delivery (Aihara and Miyazaki, 1998; Matthews et al., 1995; Nishi et al., 1996; Sukharev et al., 1992; Yoshizato et al., 2000; Zewert et al., 1995), which uses electric pulses to promote uptake of DNA. Although electroporation is of interest as an alternative to viral delivery methods, it has not yet been developed to the point that it can be applied routinely in clinical practice. One of the obstacles to further progress is the lack of a good theoretical model of the processes taking place during electroporation-mediated DNA delivery. Such a model must satisfy the following requirements:

1. The model should be able to predict the creation of macropores, i.e., pores whose radii are larger than the radius of a DNA macromolecule. The effective radius of supercoiled DNA is 5–9 nm (Rybenkov et al., 1997). Thus, one would expect that pores that admit DNA have radii of at least 10 nm, and possibly greater if the interactions of the DNA chain with the pore are of importance.
2. These pores should be stable, i.e., they should stay open for the entire time needed for the DNA chain to enter the cell. This time is expected to be on the order of milliseconds, based on experimental observations that no uptake of macromolecules is observed with pulses shorter than 1 ms (Klenchin et al., 1991; Rols and Teissié, 1998).
3. Such large and stable pores should be reversible, i.e., they should reseal without mechanical rupture of the membrane or other lethal injury to the cell. For the gene therapy to succeed, the cell must be healthy enough to express proteins coded by the DNA.

The existing theory of electroporation fails to meet these requirements. Specifically, the Smoluchowski equation (SE), which has been used to describe the biophysical mechanism of the creation and evolution of pores since the late 1970s, cannot model pores large enough to admit plasmid DNA. When the applied transmembrane potential is low (e.g., below 0.4 V), the SE predicts that very few pores will be created, and that their radii will be below 1 nm (Joshi and Schoenbach, 2000). For larger transmembrane potentials, more pores are created but they expand so rapidly that in a matter of microseconds they exceed the radius beyond which electroporation becomes irreversible even if the transmembrane potential is removed (Freeman et al., 1994; Joshi and Schoenbach, 2000). This feature of the SE is well known and has been exploited in theoretical studies of irreversible breakdown and rupture of artificial lipid bilayers (Abidor et al., 1979) and biological cells (Joshi and Schoenbach, 2000). However, experiments involving uptake of plasmid DNA by cells do not support such a catastrophic scenario. Even though pulse durations used in such studies are on the order of milliseconds, a large percentage of cells survive, and they are healthy enough to express proteins coded by DNA (Klenchin et al., 1991; Rols and Teissié, 1998; Tekle et al., 1991; Wolf et al., 1994; Xie and Tsong, 1992; Yoshizato et al., 2000; Zhang et al., 1996). To account for this discrepancy, some researchers put forward a hypothesis that DNA entry into cells relies on the DNA-membrane interactions, which may be facilitated by a collection of small, 1 nm pores (Neumann et al., 1996; Rols and Teissié, 1998; Rols et al., 1998b; Sukharev et al., 1992, 1994).

An alternative way of resolving this discrepancy is presented here: a model that may be considered a nonlinear

Submitted October 14, 2003, and accepted for publication January 21, 2004.
Address reprint requests to Wanda Krassowska, Tel.: 919-660-5105; Fax: 919-660-5405; E-mail: wanda.krassowska@duke.edu.
© 2004 by the Biophysical Society
0006-3495/04/05/2813/14 $2.00

extension of the SE and that can predict the creation of stable macropores. The next section presents the governing equations of the model, outlines their numerical implementation, and describes the DNA uptake model of Neumann et al. (1996), which was added to our electroporation model to bring simulations closer to experiments. The Results section presents a detailed example of the process of creation and evolution of macropores during and after the pulse. The following sections describe how the number and size of pores, as well as DNA uptake, depend on the magnitude and duration of the electric pulse. Finally, the model is used to predict the outcome of a two-pulse protocol, which was proposed by Sukharev et al. (1992) specifically for DNA delivery.

MODEL

Mathematical description of pore creation and evolution

Creation

According to the established theory of electroporation (Abidor et al., 1979; Glaser et al., 1988; Weaver, 1994; Weaver and Chizmadzhev, 1996), all pores are initially created hydrophobic at a rate determined by their energy (Fig. 1). Most of them are quickly destroyed by lipid fluctuations, but if hydrophobic pores of radius $r \geq r_*$ are created, they convert spontaneously to long-lived hydrophilic pores, which are of interest in this study. Thus, most hydrophilic pores are created within a small range of radii just above r_* and immediately expand to the minimum-energy radius r_m (Neu and Krassowska, 1999). For the purpose of this study, we assume that pores are created with the initial radius r_m at a rate determined by an ordinary differential equation (ODE) (DeBruin and Krassowska, 1999; Neu and Krassowska, 1999)

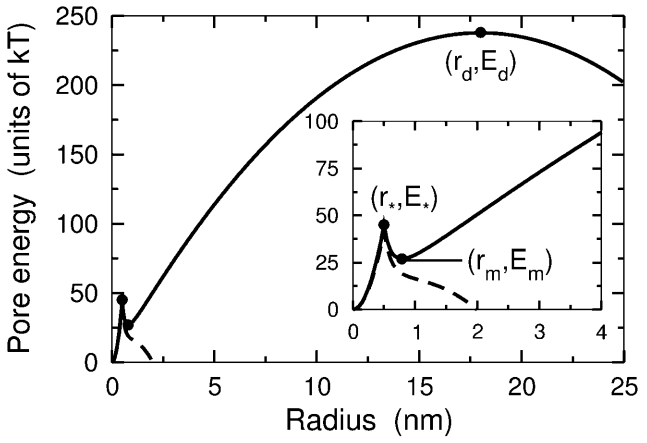

FIGURE 1 Energy of hydrophobic ($r < r_*$) and hydrophilic ($r > r_*$) pores as a function of pore radius at the transmembrane potential $V_m = 0$ (*solid lines*). The radii r_* and r_d indicate positions of energy barriers for creation of hydrophilic pores and for pore expansion, respectively, and r_m is the position of a local energy minimum. E_*, E_m, and E_d denote energy values for pores of radii r_*, r_m, and r_d, respectively. Dashed lines show pore energy for $V = 0.5$ V, illustrating that for sufficiently large V_m, local minimum and maximum disappear and any pore with the radius above r_* will grow. (*Inset*) Close-up of energy for small pores.

$$\frac{dN}{dt} = \alpha e^{(V_m/V_{ep})^2}\left(1 - \frac{N}{N_{eq}(V_m)}\right), \tag{1}$$

where N is the pore density, V_m is the transmembrane potential, V_{ep} is the characteristic voltage of electroporation, and α is the creation rate coefficient. N_{eq} is the equilibrium pore density for a given voltage V_m:

$$N_{eq}(V_m) = N_0\, e^{q\,(V_m/V_{ep})^2}, \tag{2}$$

where N_0 is the equilibrium pore density for $V_m = 0$ and $q = (r_m/r_*)^2$, with radii r_m and r_* defined in Fig. 1. Further details of the model of pore creation can be found in our previous publication (Neu and Krassowska, 1999), in which Eq. 1 is derived from the SE by a rigorous asymptotic analysis. Values of all parameters are given in Table 1.

Evolution

The pores that are initially created with radius r_m change size to minimize the energy W of the entire lipid bilayer. If at a given instant in time there exists an ensemble of K pores with radii r_j, $j = 1, \ldots, K$, then the rate of change of the radii is determined by the gradient flow of the bilayer energy

$$\frac{dr_j}{dt} = -\frac{D}{kT}\frac{\partial W}{\partial r_j}, \quad j = 1, 2, \ldots, K, \tag{3}$$

TABLE 1 Parameters of the electroporation model

Symbol	Value	Definition
α	1×10^{9} m^{-2} s^{-1}	Creation rate coefficient*
V_{ep}	0.258 V	Characteristic voltage of electroporation*
N_0	1.5×10^{9} m^{-2}	Equilibrium pore density at $V_m = 0$*
r_*	0.51×10^{-9} m	Minimum radius of hydrophilic pores†
r_m	0.8×10^{-9} m	Minimum energy radius at $V_m = 0$ V†
D	5×10^{-14} m^2 s^{-1}	Diffusion coefficient for pore radius‡
T	310 K	Absolute temperature (37°C)
β	1.4×10^{-19} J	Steric repulsion energy§
γ	1.8×10^{-11} J m^{-1}	Edge energy†,‡
σ_0	1×10^{-3} J m^{-2}	Tension of the bilayer without pores‡
σ'	2×10^{-2} J m^{-2}	Tension of hydrocarbon-water interface¶
A	1.26×10^{-9} m^2	Total area of lipid bilayer ($A = 4\pi a^2$, assuming spherical cell of radius $a = 10$ μm)
F_{max}	0.70×10^{-9} N V^{-2}	Maximum electric force for $V_m = 1$ V‖
r_h	0.97×10^{-9} m	Constant in Eq. 6 for electric force‖
r_t	0.31×10^{-9} m	Constant in Eq. 6 for electric force‖
C_m	9.5×10^{-3} F m^{-2}	Surface capacitance of the membrane*
R_m	0.523 Ω m^2	Surface resistance of the membrane*
R_s	100 Ω	Series resistance of the experimental setup**,‡
h	5×10^{-9} m	Membrane thickness†
g	2 S m^{-1}	Conductivity of the solution (Tyrode's)††

*DeBruin and Krassowska (1999).
†Glaser et al. (1988).
‡Freeman et al. (1994).
§Neu and Krassowska (1999).
¶Israelachvili (1992).
‖Neu et al. (2003).
**Chernomordik et al. (1983).
††Weidmann (1970).

where D is the diffusion coefficient of the pore radius, k is the Boltzmann constant, and T is the absolute temperature. The bilayer energy W is

$$W = \sum_{j=1}^{K} \left\{ \beta \left(\frac{r_*}{r_j} \right)^4 + 2\pi\gamma r_j - \pi\sigma_{\text{eff}}(A_p) r_j^2 + \int_0^{r_j} F(r_j, V_m) dr \right\}. \quad (4)$$

In Eq. 4, the first term accounts for the steric repulsion of lipid heads; the second, for the edge energy of the pore perimeter; the third, for the effect of pores on the membrane tension; and the fourth, for the contribution of the transmembrane potential. All parameters are defined in Table 1.

There are two differences between our model and those published previously. First, the third term in Eq. 4 contains the effective tension of the membrane, σ_{eff}, in place of a constant parameter σ_0, which represents the tension of a membrane without pores. σ_{eff} is a function of the combined area of pores, $A_p = \sum_{j=1}^{K} \pi r_j^2$:

$$\sigma_{\text{eff}}(A_p) = 2\sigma' - \frac{2\sigma' - \sigma_0}{(1 - A_p/A)^2}, \quad (5)$$

where σ' is the energy per area of the hydrocarbon-water interface (Israelachvili, 1992) and A is the total area of the lipid bilayer. The use of σ_{eff} instead of σ_0 introduces tension coupling between pores: as pores are created and expand, their total area A_p increases, decreasing the membrane tension σ_{eff} ''felt'' by each pore. Eventually, the decrease in σ_{eff} halts further expansion of pores. Thus, it is the presence of σ_{eff} in Eq. 4 and its dependence on A_p that allows our model to predict stable pores with radii of tens of nanometers. Further details can be found in our previous publication (Neu and Krassowska, 2003), in which the coupling of pores through membrane tension seen in Eq. 4 is related to a nonlinear generalization of the SE, and the equation governing the evolution of pores (Eq. 3) is derived from this nonlinear SE by a rigorous asymptotic analysis.

The second difference is the revision of the contribution of the transmembrane potential V_m to the bilayer energy (last term in Eq. 4). Assuming that the inner surface of a pore is toroidal (Kandušer et al., 2003), as illustrated in the inset to Fig. 2, $F(r, V_m)$, the electric force acting on a pore is given by a formula

$$F(r, V_m) = \frac{F_{\max}}{1 + \dfrac{r_h}{r + r_t}} V_m^2, \quad (6)$$

where $F_{\max}$, r_h, and r_t are constants. Equation 6 predicts that the force F approaches a constant value $F_{\max}$ as the pore radius increases (Fig. 2). This is different from the formulas used previously, which predicted that the electrical force either increased linearly (Abidor et al., 1979) or decreased to zero (Barnett and Weaver, 1991; Joshi et al., 2002; Pastushenko and Chizmadzhev, 1982) with the increase in the pore radius. Previous formulas apply only to small pores with the cylindrical inner surface, whereas Eq. 6 applies to toroidal pores of arbitrary size. Further details can be found in our previous publication (Neu et al., 2003), in which the electrical force F acting on a pore is derived from first principles and computed numerically, and Eq. 6 arises as a heuristic approximation of the numerical solution.

Transmembrane potential

As pores are created according to Eq. 1 and their radii evolve according to Eq. 3, their presence affects the transmembrane potential V_m. To compute the value of V_m at each time step, one must choose what type of experimental preparation to model. This study uses the simplest one, i.e., a uniformly polarized membrane. Its circuit representation in Fig. 3 contains current I_p through electropores, capacitance $C = C_m A$ and resistance $R = R_m/A$, where C_m and R_m are surface capacitance and surface resistance of the membrane, respectively. The stimulus takes the form of a voltage V_0 that is applied to the membrane through a resistor R_s, which represents the series resistance of the experimental setup.

Thus, the transmembrane potential V_m is governed by an ODE,

$$C\frac{dV_m}{dt} + \left(\frac{1}{R_s} + \frac{1}{R} \right) V_m + I_p = \frac{V_0}{R_s}, \quad (7)$$

where $I_p = \sum_{j=1}^{K} i_p(r_j, V_m)$ is the combined current through all pores. The current-voltage relationship for an individual pore,

$$i_p(r, V_m) = \frac{V_m}{R_p + R_i}, \quad (8)$$

assumes that voltage drop V_m occurs across the sum of the pore resistance, $R_p = h/(\pi g r^2)$, and the input resistance, $R_i = 1/(2gr)$ (Newman, 1966), where h is the membrane thickness and g is the conductivity of the solution. Because this study focuses on large pores, the pore resistance R_p is assumed

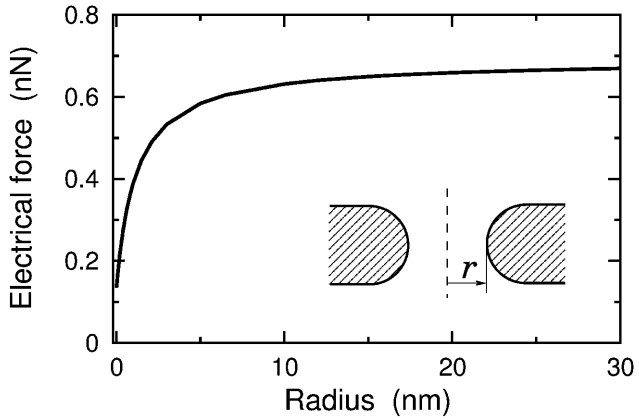

FIGURE 2 Electrical force $F(r, V_m)$ acting on a pore, given by Eq. 6, with $V_m = 1$ V. (*Inset*) Assumed geometry of a hydrophilic pore.

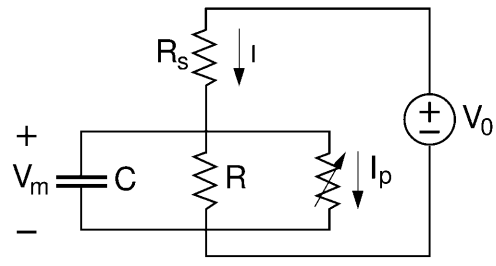

FIGURE 3 Circuit representation of a uniformly polarized membrane considered in this study. Capacitor C represents the total capacitance of the membrane and the constant resistor R accounts for the flow of current through channel proteins. The variable resistor accounts for the dynamically changing current through pores, I_p. Resistor R_s represents the series resistance of the experimental setup and V_0 is the external stimulus.

ohmic and the interactions between ions and the pore wall (Barnett and Weaver, 1991; Pastushenko and Chizmadzhev, 1982) are ignored (they are of importance only for pores smaller than ≈5 nm). Equation 7 is used with the initial condition $V_m = 0$, i.e., the rest potential of the cell is ignored. An abrupt increase of the current I_p when V exceeds threshold is due to creation of pores (in the model represented by the increase of the number of pores K) and the expansion of their radii (which in the model decreases resistances R_p and R_i).

Resealing

When the electric pulse is turned off, the membrane discharges very rapidly through the existing pores, V_m drops to zero, and the pores shrink to near the minimum-energy radius r_m. Once pores become that small, they can reseal by converting to a hydrophilic configuration and being destroyed by lipid fluctuations. The resealing process is already included in Eq. 1: after the pulse has created a certain number of pores, the pore density N is larger than N_0, the equilibrium pore density for $V_m = 0$. Hence, the right-hand side of Eq. 1 is negative and the pore density N decreases. With the parameters from Table 1, the time constant of resealing is ~3 s (Glaser et al., 1988).

Note that only pores that have shrunk to a radius near r_m participate in resealing. If there exist any macropores with $r \gg r_m$, they cannot reseal by the mechanism represented in Eq. 1. The resealing of these giant pores is beyond the scope of this model because it involves such processes as a change in cell volume (Sandre et al., 1999) or active, exocytotic rebuilding of the lipid bilayer (McNeil and Steinhardt, 1997).

Numerical implementation

The model described by Eqs. 1–8 has been implemented using MATLAB. An important feature of this implementation is that it represents two populations of pores in two different ways. Small pores, whose radii congregate near the minimum-energy radius r_m, are accounted for by a pore density $N(t)$. All pores in this population are assumed to have the same radius r_m, and $N(t)$ increases or decreases according to Eq. 1. Large pores, whose radii are larger than r_m, are represented individually: the radius of each pore evolves according to Eq. 3. The program accounts for the exchange of pores between these two populations.

For a typical simulation, initial conditions assume an intact membrane and no transmembrane potential. Thus, $V_m(0) = 0$, $N(0) = N_0$ (i.e., there is an equilibrium pore density at $r = r_m$), and $K = 0$ (i.e., there are no large pores). The time loop contains the following steps:

- Create pores. Use Eq. 1 to compute pores created or resealed in this time step. Increase or decrease $N(t)$ accordingly.
- Launch pores. If the right-hand side of Eq. 3 evaluated at $r_j = r_m$ is positive, the energy minimum at r_m no longer exists (Fig. 1, *dashed line*) and no pores accumulate there. However, as a result of the creation step, $N(t)$ may hold some pores (i.e., $N(t)\,A > 1$); these pores should be ''launched'' and allowed to grow. To do so, K is increased by an integer number of pores, floor($N(t)\,A$), and $N(t)$ is decreased by a corresponding value. To ensure that pore radii are numerically distinct, the launched pores are assigned radii with a normal distribution about r_m with a standard deviation of 0.001 nm.
- Compute effective membrane tension. Using the density $N(t)$ of small pores and the radii r_j, $j = 1, \ldots, K$ of large pores, compute the total pore area A_p and, from Eq. 5, the effective membrane tension σ_{eff}.
- Update pore radii. For every pore in the large-pore population, use Eq. 3 to update its radius r_j, $j = 1, \ldots, K$.
- Absorb pores. If any radius r_j from the large pore population has fallen below r_m as a result of the previous step (which occurs when pores are shrinking), this pore needs to be ''absorbed'' into the small-pore population. Hence, K is decreased by 1 and $N(t)$ is increased by $1/A$.
- Update transmembrane potential. Using the density $N(t)$ of small pores and the radii r_j, $j = 1, \ldots, K$ of large pores, compute current through each pore from Eq. 8 and the total current I_p. Use Eq. 7 to compute the new value of $V_m(t)$.

The numerical integration of Eqs. 1, 3, and 7 is performed using MATLAB function ode23t. The initial time step is 10 ps, but an adaptive time-stepping algorithm increases the time step as the simulation progresses to decrease the total run time. The run time depends on the number of large pores created by the pulse. Stronger pulses, which create more than 10^4 pores, result in unacceptably long runs. To decrease run times in such cases, the program launches groups of pores rather than individual pores. All pores in the group are assumed to have the same radius, and the program keeps track of the number of pores in each launched group. For example, the simulation presented in Fig. 4, in which a 1.25 V, 10 ms pulse created 40,057 large pores, took 3 min to run on a Sun Blade 1000 (750 MHz) work station with pores launched in groups.

Modeling uptake of DNA

The model described thus far can predict the number of pores and their sizes during an arbitrary pulsing protocol. Although important, these predictions are not directly comparable to DNA uptake experiments, which typically measure the fraction of transformed cells. To bring the model one step closer to experiments, we have extended the model described above by including the uptake of the DNA by the cell. Specifically, we use a modification of a model proposed by Neumann et al. (1996) for the uptake of the YEp 351 plasmid DNA by yeast cells. The uptake of the DNA is described by the Nernst-Planck equation, which accounts for both the diffusive and electrophoretic transport:

$$\frac{d[DNA]_i}{dt} = -\frac{D_0}{hV_{cell}}\,S(t) \times \left\{[DNA]_i - [DNA]_o\left(1 + \frac{|z_{eff}|e}{kT}\,V_p(t)\right)\right\}, \quad (9)$$

where $[DNA]_i$ and $[DNA]_o$ are concentrations of DNA inside and outside the cell, respectively, D_0 is the DNA diffusion coefficient, V_{cell} is the cell volume, z_{eff} is the effective valence of the DNA molecule, and e is the elementary charge. The two functions of time are the pore area $S(t)$ and the voltage drop across the pore $V_p(t)$.

Equation 9 differs from Eq. 12 in Neumann et al. (1996) in that it follows a slightly different notation and incorporates both influx and efflux of DNA from the cell. In addition, Neumann et al. used their Eq. 12 for the entire cell membrane, so that $S(t)$ was the combined area of all pores and $V_p(t)$ was equal to the transmembrane potential $V_m(t)$, measured away from the pore. In contrast, we apply Eq. 9 to each individual pore (provided its radius r is above that of the supercoiled DNA, 10 nm (Rybenkov et al., 1997)), and hence $S(t)$ is the area of one pore, evaluated at each time step by our electroporation model. $V_p(t)$ is also evaluated at each time step, but in our model it represents only the fraction of $V_m(t)$ that corresponds to an actual voltage drop across the pore:

$$V_p(t) = \frac{V_m(t)}{1 + R_i/R_p}, \quad (10)$$

where R_p and R_i are pore resistance and input resistance defined below Eq. 8.

Other parameters of Eq. 9 were chosen as follows:

1. The value of D_0 of 2.5×10^{-10} m^2/s used by Neumann et al. (1996) is too large for the 5.6 kb pair YEp 351 plasmid, even if measured in water, and it does not reflect that the movement of DNA slows down inside the pore. Evaluated from the molecular weight (Fournier, 1998),

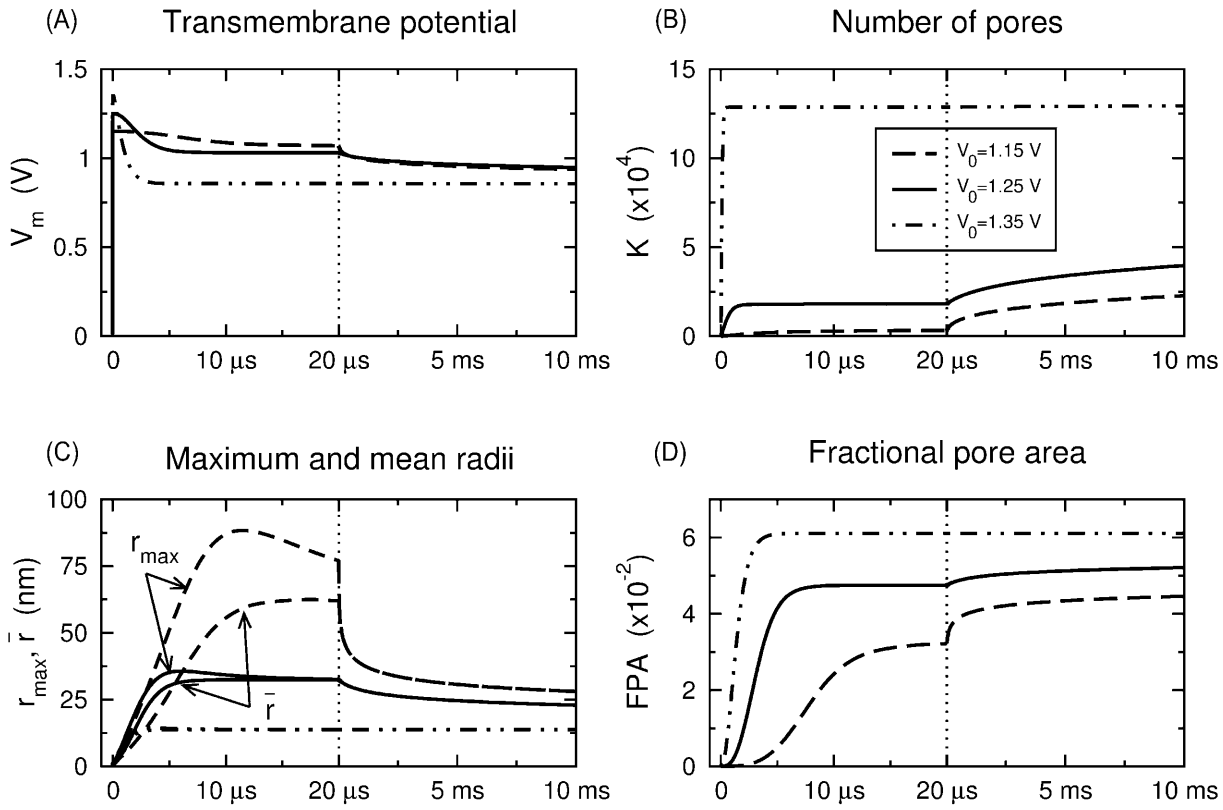

FIGURE 4 Creation and evolution of pores. A 10 ms pulse was applied at three strengths: 1.15 V (*dashed line*), 1.25 V (*solid line*), and 1.35 V (*dash-dotted line*). The left side of each panel shows the initial transient (0–20 μs) and the right side shows the long time evolution (20 μs–10 ms). (*A*) Transmembrane potential V_m. Note that the final value of V_m does not depend monotonically on the pulse strength. (*B*) The number of large pores K. K levels off for the 1.35 V pulse, indicating that the creation of pores effectively stopped. For 1.15 and 1.25 V pulses, K appears to level off on the microsecond timescale; on the millisecond scale, it continues to slowly increase during the remainder of the pulse at a rate that decreases monotonically with decreasing V_m. (*C*) Maximum radius r_{max} and mean radius $\bar{r}$. The difference between r_{max} and $\bar{r}$ illustrates the distribution of pores: initially, pore radii are spread out, then all pores assume the same size. For the 1.35 V pulse, only one line is visible because r_{max} and $\bar{r}$ nearly overlap. Note the decrease of final radius with the pulse strength. (*D*) Fractional pore area, FPA.

D_0 for YEp 351 DNA in water is 9.8×10^{-12} m^2/s. Assuming a sevenfold decrease inside the pore (Ambjörnsson et al., 2002), we used $D_0 = 1.3 \times 10^{-12}$ m^2/s.

2. Neumann et al. used in their calculation $z_{eff} = -1$, an effective valence of the phosphate group. We used z_{eff} of the entire YEp 351 DNA, which we computed from the Einstein's formula (Plonsey and Barr, 1988)

$$\mu = D_0 \frac{|z_{eff}|e}{kT}, \tag{11}$$

which relates mobility μ and diffusion coefficient D_0. For YEp 351 DNA in water, $\mu = 10^{-8}$ m^2/(Vs) (Neumann et al., 1996), $D_0 = 9.8 \times 10^{-12}$ m^2/s (see above), and therefore $z_{eff} = -27$.

3. Concentration of DNA outside cells was assumed constant. According to Neumann et al., the DNA uptake is proportional to the DNA bound to the membrane rather than the total DNA. Hence, we used $[DNA]_o = 1.3 \times 10^{-6}$ mol/m^3, which corresponds to the fraction of bound DNA for a total DNA concentration of 2.7×10^{-6} mol/m^3 (Fig. 1 in Neumann et al., 1996).
4. All calculations assume a spherical cell with a 10 μm radius.

To compute DNA uptake, the program has been extended by including in each time step the computation of DNA transport through each pore by integrating numerically Eq. 9. Only pores of radii $r > 10$ nm are assumed to be permeable to DNA. The uptakes for all pores are summed and divided by two to account for the fact that negatively charged DNA molecules enter predominantly through the depolarized half of the cell (Klenchin et al., 1991). The resulting intracellular DNA concentration, $[DNA]_i$, is reported relative to the threshold concentration required for the cell transformation given by Neumann et al., $[DNA]_{th} = 1.7 \times 10^{-7}$ mol/m^3.

RESULTS

Creation and evolution of macropores predicted by the model

Fig. 4 shows the simulation of typical electroporation experiments, in which electric pulses of 10 ms duration are applied. Let us consider the pulse of strength $V_0 = 1.25$ V (Fig. 4, *solid line*). After the pulse is turned on, transmembrane potential V_m jumps to the applied voltage (Fig. 4 *A*). With V_m above threshold, the number of pores increases dramatically (Fig. 4 *B*) because of the exponential dependence of the creation rate on V_m^2 (Eq. 1). The nascent

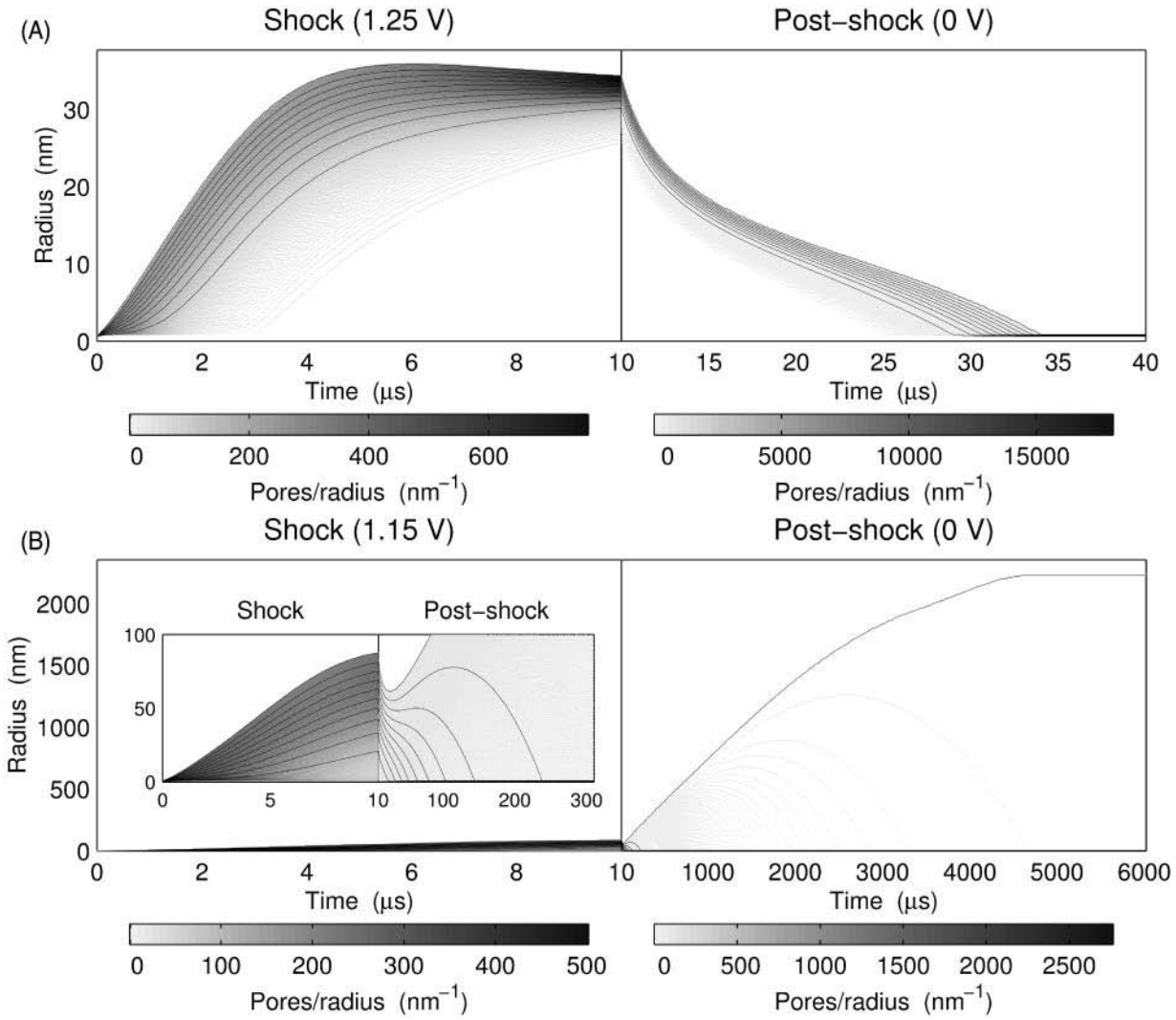

FIGURE 5 The pore radii during the 10 μs pulse and the postshock evolution of pores. The gray scale represents the pore radii distribution (i.e., the number of pores with radii between r and $r + dr$). Solid lines show the 10, 20, . . . , 100th percentiles of the maximum pore radius, illustrating the evolution of the pore radii in time. (*A*) Evolution of pores after a 1.25 V pulse, which created 18,025 pores. After the pulse, all pores shrink to r_m (the minimum-energy radius of Fig. 1). (*B*) Evolution of pores after a 1.15 V pulse, which created a smaller number of pores, 2772. After the pulse, all pores shrink to r_m except the largest pore, which grows to a stable radius of 2.23 μm. (*Inset*) The pulse and the first 300 μs after the pulse shown on an expanded vertical scale.

pores grow rapidly (Fig. 4 *C*; see also the *left panel* of Fig. 5 *A*, which shows the first 10 μs of this pulse) because of the high effective membrane tension and the large electric force on the pores, which depends on V_m^2 (Eq. 6). The creation and growth of pores cause the fractional pore area (FPA $\equiv A_p/A$) to increase (Fig. 4 *D*).

This period of rapid creation and expansion cannot be sustained because the electroporation decreases the electrical resistance of the membrane, decreasing V_m (Fig. 4 *A*), and slowing the creation rate (Fig. 4 *B*) and the expansion rate of small pores (Fig. 4 *C* and Fig. 5 *A*, *left panel*). Additionally, the effective membrane tension is reduced, decreasing and eventually reversing the expansion rate of the pores. With larger pores shrinking and small, newly created pores expanding, all pores eventually accumulate at the same radius of 34.4 nm (Fig. 4 *C* and Fig. 5 *A*, *left panel*).

For the 1.25 V pulse, V_m remains sufficiently large (near 0.9 V) for the creation of pores to continue, causing the transmembrane potential and accumulation radius to decrease slowly in time (Fig. 4, *A* and *C*) and the number of pores to increase (Fig. 4 *B*). FPA also increases slightly as the combined area of new pores is greater than the pore area lost by the decrease in the accumulation radius (Fig. 4 *D*). If the applied voltage is larger (e.g., 1.35 V in Fig. 4), more pores are created, V_m decreases well below threshold, and the creation rate decreases to a very small value. Thus, for sufficiently large pulses, the accumulation radius, transmembrane potential, fractional pore area, and number of pores remain effectively constant after the initial transient.

Postshock evolution of macropores and cell survival

Once the pulse is turned off and the membrane discharges, so that $V_m \approx 0$, the population of pores can evolve according to two different scenarios: shrinkage or coarsening (Neu and Krassowska, 2003). These are illustrated in Fig. 5 for 10 μs pulses of strengths 1.25 V (Fig. 5 *A*) and 1.15 V (Fig. 5 *B*). In shrinkage, all pores decrease their radii to the minimum energy radius r_m (Fig. 5 *A*). Shrinkage occurs when the pulse is sufficiently strong and long to create a large number of pores, i.e., K must exceed a critical value $K_c \approx \sigma_0^3 A/(27\pi\sigma'\gamma^2)$ (for all pores accumulated at the same radius (Neu and Krassowska, 2003)). If a weaker or shorter pulse creates a number of pores below K_c, coarsening occurs. In coarsening, one pore expands to a radius of 2.23 μm (for a cell of 10 μm radius), whereas all other pores shrink to r_m (Fig. 5 *B*). Coarsening and shrinkage may correspond to irreversible and reversible breakdown, respectively, since the former has been observed to occur at lower pulse strengths than the latter (Benz et al., 1979; Weaver and Chizmadzhev, 1996).

From the viewpoint of cell survival, shrinkage is preferable, as pores of radii near r_m readily reseal (Eq. 1). Coarsening creates a giant, 2.23 μm pore, leaving the cell vulnerable to leakage and death. Thus, it is important to use pulses sufficiently strong and long enough to avoid the postshock coarsening.

Effects of pulse magnitude and duration

The pore population depends on the magnitude and duration of the electric pulse applied to the membrane (Tekle et al., 1991; Wolf et al., 1994) and the model is used to explore this dependence. Table 2 lists simulation results for 10 ms pulses of seven magnitudes, ranging from $V_0 = 0.8$ V to 1.4 V.

The number of large pores, K, measured at the end of the pulse (10 ms) increases with the pulse strength. There is no sharp threshold for electroporation (Glaser, 1986; Sukharev et al., 1994): as expected from Eq. 1, each of the pulses listed in Table 2 creates some pores. However, not all these pulses will be recognized as electroporating in experiments, which typically identify electroporation by the uptake of small molecules (Gabriel and Teissié, 1997) or the decrease in V_m during the pulse (Benz and Zimmermann, 1980; Hibino et al., 1991; Powell et al., 1989). Using the latter criterion and assuming that a 5% decrease is experimentally detectable, 0.8 and 0.9 V pulses will be considered subthreshold, and 1 V and larger pulses, suprathreshold.

K appears to be still increasing at the end of pulses with $V_0 \leq 1.3$ V but not for stronger pulses (1.35 V pulse in Fig. 4 *B*, millisecond timescale). Strictly speaking, K is increasing for all pulses, but if the number of pores created within 1 μs is $<10^{-6}$ times the number of existing pores, we consider the creation process terminated. This is why K is considered still increasing for the 0.8 V pulse but not for the 1.4 V pulse, even though final V_m is nearly identical for these two pulses.

The distribution of pore radii is characterized by the maximum radius r_{max} and the mean radius $\bar{r}$. These both decrease with the pulse magnitude, indicating that stronger pulses create more but smaller pores. The decrease in pore radii does not quite compensate for the increase in the number of pores, and thus the fractional pore area, FPA, increases approximately linearly with the pulse strength. The difference between r_{max} and $\bar{r}$ quantifies how wide the pore population is. For weak pulses, there is a large difference between r_{max} and $\bar{r}$ during the initial transient (Table 2 and Fig. 4 *C*, microsecond scale) but on the millisecond scale, r_{max} and

TABLE 2 Effects of pulse magnitude on pore creation and evolution

V_0 (V)		0.8	0.9	1.0	1.1	1.2	1.3	1.4
K ($\times 10^3$)	10 ms*	0.162	1.28	6.01	15.9	30.5	56.8	303
K increasing†	10 ms	Yes	Yes	Yes	Yes	Yes	Yes	No
V_m (V)	Max	0.800	0.900	1.00	1.10	1.20	1.30	1.40
	10 ms	0.790	0.865	0.907	0.929	0.943	0.936	0.766
r_{max} (nm)	Max	1900	1280	326	144	55.7	22.6	9.41
	10 ms	197	82.8	45.7	32.0	25.2	19.9	9.18
$\bar{r}$ (nm)	Max	1430	432	241	83.0	46.4	21.4	9.18
	10 ms	197	82.8	45.7	32.0	25.2	19.9	9.18
FPA ($\times 10^{-2}$)	10 ms	1.58	2.20	3.14	4.05	4.84	5.61	6.39
$[DNA]_i/[DNA]_{th}$	10 ms	0.432	1.40	3.39	5.27	6.43	7.19	0
Postshock‡	>10 ms	Coarse	Coarse	Shrink	Shrink	Shrink	Shrink	Shrink

*The second column specifies whether the quantity is measured at its maximum (Max), at the end of the pulse (10 ms), or after the pulse (>10 ms).
†K is considered increasing if the number of pores launched within 1 μs exceeds 10^{-6} times the number of existing large pores.
‡Coarse and shrink denote postshock coarsening and shrinkage, respectively.

TABLE 3 Effects of pulse duration on pore creation and evolution

Duration (ms)	$V_0 = 1.15$ V				$V_0 = 1.35$ V			
	0.01	0.1	1	10	0.01	0.1	1	10
K ($\times 10^3$)	2.76	5.07	11.1	22.7	129	129	129	129
K increasing	Yes	Yes	Yes	Yes	No	No	No	No
V_m (V)	1.09	1.04	0.995	0.936	0.856	0.856	0.856	0.856
r_{max} (nm)	87.0	53.4	38.2	28.1	13.9	13.8	13.8	13.7
$\bar{r}$ (nm)	55.6	52.8	38.2	28.1	13.8	13.8	13.8	13.7
FPA ($\times 10^{-2}$)	2.42	3.54	4.03	4.46	6.11	6.11	6.11	6.11
$[DNA]_i/[DNA]_{th}$	0.00159	0.0528	0.769	5.93	0.0251	0.287	2.46	7.49
Postshock	Coarse	Shrink	Shrink	Shrink	Shrink	Shrink	Shrink	Shrink

$\bar{r}$ are equal, indicating that all pores have accumulated at the same radius. For strong pulses, above 1.3 V, r_{max} and $\bar{r}$ are very close even during the initial transient, indicating that the pore population is very compact from the beginning (Table 2 and Fig. 4 *C*).

Table 3 lists simulation results for pulses of different durations, from 10 μs to 10 ms. Two pulse strengths were examined: a just subthreshold pulse (1.15 V) and the largest pulse still resulting in DNA uptake (1.35 V). The results show that the number of pores, K, radii r_{max} and $\bar{r}$, and the fractional pore area, FPA, depend on pulse duration only for weak pulses. For strong pulses, the initial transient is below 10 μs, so there is little dependence of K, r_{max} and $\bar{r}$, and FPA on the duration.

Finally, Tables 2 and 3 show that 10 ms suprathreshold pulses, 1 V or larger, are always followed by the postshock shrinkage of all pores to r_m. However, Table 3 shows that weak pulses (1.15 V) must last at least 100 μs to create enough pores to avoid coarsening and to increase the chances of the cell survival.

Uptake of DNA predicted by the model

Tables 2 and 3 also list the intracellular concentration of DNA (relative to $[DNA]_{th}$) at the end of the pulse. Sufficient DNA uptake can occur even with a slightly subthreshold pulse (0.9 V) and increases with pulse strength. For any pulse strength, the DNA uptake increases with the pulse duration (Table 3). However, DNA uptake for short pulses (10 and 100 μs) is insufficient to result in cell transformation and thus would not be detected experimentally. Pulses of millisecond duration are needed for cell transformation, a result that agrees with experimental evidence (Klenchin et al., 1991; Rols and Teissié, 1998). The uptake stops abruptly at pulses above 1.4 V because the pores created by such strong pulses are smaller than the assumed radius of the DNA, 10 nm (Table 2).

More comprehensive results on DNA uptake are presented in Fig. 6, which shows the level curves (*solid lines*) of relative DNA concentration for durations up to 10 ms and pulse strengths up to 1.4 V. The model predicts that cell transformation will be observed only for pulse parameters inside the region enclosed by bold lines. The upper boundary of this region is a horizontal line corresponding to 1.4 V: no DNA uptake occurs above this line because stronger pulses create pores too small to be permeable to DNA (see also Table 2). The lower boundary is the strength-duration relationship for cell transformation (Fig. 6, *line* labeled *1*).

Fig. 6 shows that substantial DNA uptake occurs within a relatively small range of pulse strengths, e.g., 0.87–1.4 V for the 10 ms pulse. Note that part of this range lies in the region of postshock coarsening (below the *dashed line*), so even if the DNA uptake is adequate, the cell may not survive. Thus, the usable range may be even smaller, e.g., 0.94 V–1.4 V for the 10 ms pulse.

Simulations of the two-pulse protocol

Sukharev et al. (1992) proposed a two-pulse protocol specifically for gene delivery applications. The authors argued that the first pulse, large in magnitude and short in

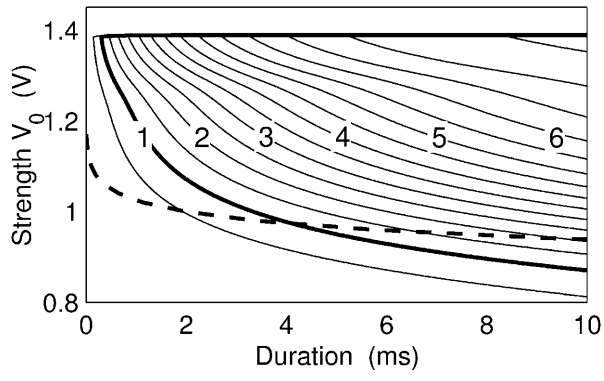

FIGURE 6 The dependence of DNA uptake on pulse magnitude and duration. Solid lines show intracellular DNA concentration normalized by the DNA concentration required for transformation. The dashed line is the boundary between postshock coarsening (*below*) and shrinkage (*above*). An effective pulse for DNA delivery should have a magnitude and duration within the region enclosed by heavy solid lines and above the dashed line (coarsening/shrinkage boundary).

duration, will quickly produce a large number of pores, whereas the second pulse, small in magnitude and longer in duration, will maintain large pore radii and will facilitate electrophoretic movement of DNA into the cell. There was a break of variable duration between the two pulses. Their experiments, as well as the study by Satkauskas et al. (2002), have confirmed that the uptake of DNA for the two-pulse protocol exceeded that for a single pulse.

The model was used to investigate the mechanism behind the greater efficiency of the two-pulse protocol. Fig. 7 *A* shows the distribution of pore radii during the 1.25 V, 10 μs first pulse, during the first 30 μs of the 100 ms break, and during the first 70 μs of the 0.5 V, 100 ms second pulse. By the end of the first pulse, 18,025 pores were created and started to accumulate at a radius of ~34 nm. During the break, all of these pores shrank to radius r_m and the resealing process started, which decreased the number of pores to 17,906 by the end of the break. During the second pulse, all of the remaining pores expanded to a radius of 18.2 nm and remained stable for the duration of the pulse. Thus, the second pulse facilitated entry of DNA into the cell by keeping the pore radii sufficiently large and by exerting an electric force on the DNA in a direction perpendicular to the membrane.

The simulation shown in Fig. 7 *B* used a slightly smaller first pulse of 1.15 V. This pulse created 2772 pores, a number small enough to trigger the coarsening process during the break (first 6 ms shown), resulting in 2771 pores at r_m and one giant pore at 2.23 μm. The resealing was considerably slower: by the end of the break, only 11 pores resealed. During the second pulse (first 1 ms shown), all the pores, including the giant one, were brought to a common radius of 45.8 nm. For both strengths, all pores shrank to r_m after the second pulse.

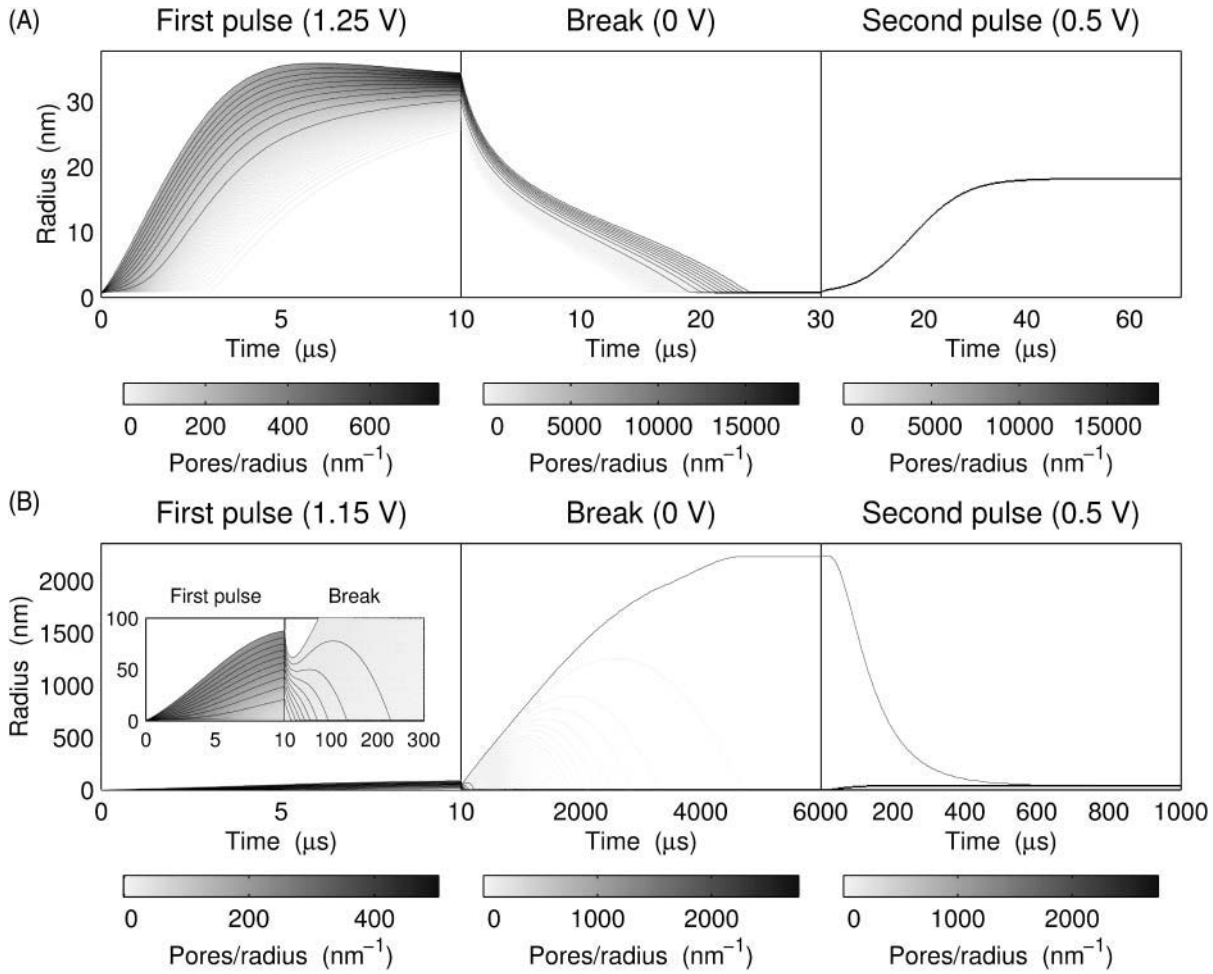

FIGURE 7 Pore evolution during the two-pulse protocol. A 10 μs first pulse was followed by a 100 μs break and then a 10 ms, 0.5 V second pulse. The gray scale and solid lines are as in Fig. 5. In each subpanel, time is measured from the beginning of the pulse or the break, respectively. (*A*) A 1.25 V first pulse; only the first 30 μs of the break and the first 70 μs of the second pulse are shown. During the break, all pores shrink to r_m. During the second pulse, all pores expand to 18.2 nm. (*B*) A 1.15 V first pulse; only the first 6 ms of the break and the first 1 ms of the second pulse are shown. During the break, all pores shrink to r_m except the largest pore, which reaches a stable radius of 2.23 μm. During the second pulse, all pores expand to 45.8 nm. (*Inset*) The first pulse and the beginning of the break shown on an expanded vertical scale.

The simulations of Fig. 7 suggest that the two-pulse protocol allows control of the number and size of pores during the second pulse. The number of pores is determined by the magnitude of the first pulse but it can be decreased to a desired number by changing the duration of the break between pulses. The pore size can be increased in three different ways: by decreasing the magnitude of the first pulse (fewer pores will be created and they will expand to larger radii), by increasing the break between pulses (more pores will reseal), and by increasing the magnitude of the second pulse. Although there are limits on how much the pulse strength can be manipulated, the two-pulse protocol gives better control of pore size and, by allowing very long durations of the second pulse, increases the DNA uptake with less of an effect on cell viability. This combination of properties may be responsible for the effectiveness of the two-pulse protocol in achieving high transfection efficiencies.

Additional simulations were performed to examine qualitative agreement between the model and the experiment. Quantitative comparison is not possible because the exact relationship between DNA uptake (predicted by the model) and transfection efficiency (measured experimentally) is not known. Fig. 8 *A* shows the intracellular DNA concentration as a function of the second pulse duration. The monotonic, nearly linear increase of DNA concentration is qualitatively similar to the results reported in Fig. 5 of Sukharev et al. (1992), although the initial nonlinear part is more pronounced in the experiment. This difference may come from the fact that the experiment used decaying exponential rather than rectangular pulses.

Fig. 8 *B* shows DNA concentration as a function of the break duration. In both the model and the experiment (Fig. 6 of Sukharev et al., 1992), DNA uptake and transformation efficiency decrease in a sigmoidal fashion. However, only a part of the sigmoidal curve is seen in the experiment for the same range of break durations. The difference is due to the model parameters not corresponding to the cell type used in the experiment, but the agreement can be improved by choosing a longer time constant for resealing.

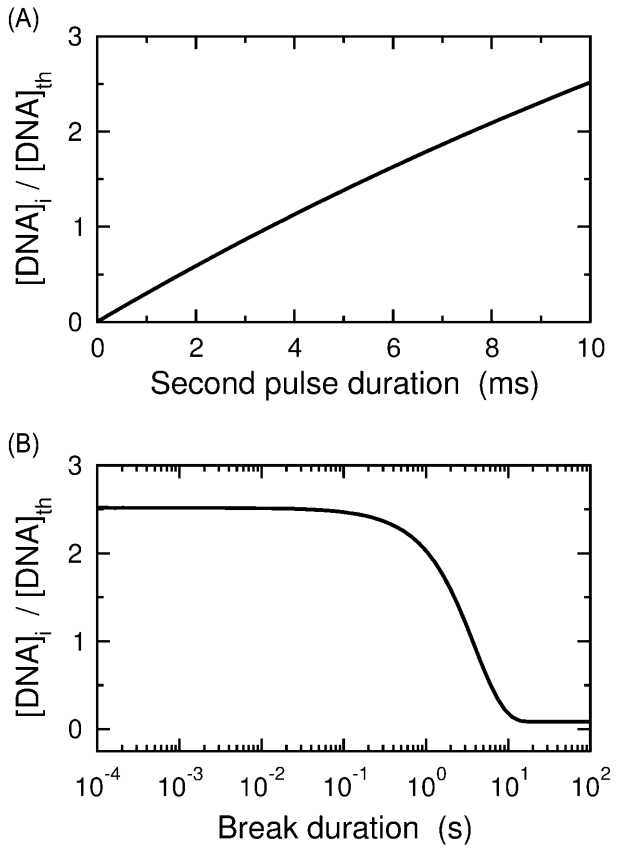

FIGURE 8 DNA uptake during the two-pulse protocol. A 10 μs, 1.25 V first pulse is followed by a break and then a 0.5 V second pulse. (*A*) Uptake as a function of the second pulse duration. The preceding break was 100 μs. (Note that the corresponding Fig. 5 in Sukharev et al. (1992) reported electric charge as a measure of pulse duration, because their pulse was not rectangular.) (*B*) Uptake as a function of break duration. The second pulse duration was 10 ms.

DISCUSSION

Limitations and future work

In this study, our model of the creation and evolution of pores is used only in the context of a uniformly polarized membrane patch (Eq. 7). Following other studies, we interpret the circuit of Fig. 3 as an idealized representation of a depolarized (or hyperpolarized) ''polar'' region of a single cell exposed to an external field (Gowrishankar and Weaver, 2003; Joshi and Schoenbach, 2000). It is in these regions of the cell that the transmembrane voltage is the largest and most pores are created (Hibino et al., 1991). Thus, these regions are also most important to gene delivery. Relating the circuit model of Fig. 3 to a spherical cell of radius a, V_0 can be interpreted as the maximum transmembrane potential induced in a cell by the external electric field E: $V_0 = 1.5\ E\ a$.

Even though electroporation in cells is fundamentally the same as in membranes (Chernomordik et al., 1987), some differences are expected. In contrast to a uniformly polarized membrane, V_m in a cell varies with the position (Hibino et al., 1991; Pavlin and Miklavčič, 2003), and the number of pores and their sizes are expected to vary as well. This leads to an important difference in the behavior of a patch versus a cell. In an electroporated patch, V_m decreases considerably below threshold, even to almost zero if the pulse is sufficiently strong (see Benz and Zimmermann, 1980, for experimental evidence and Barnett and Weaver, 1991, for modeling results). Such a drastic decrease does not occur in a cell, where the adjacent nonelectroporated regions maintain V_m at an approximately threshold level, even for very strong shocks (see Hibino et al., 1991, for experimental evidence and DeBruin and Krassowska, 1999, for modeling results).

This drop in V_m occurring in a membrane patch is the reason why our study could not reproduce the exact electrical conditions of the two-pulse experiment of Sukharev et al. (1992). In both the experiment and the model, the second pulse was chosen to be approximately half of the threshold, but the ratio of the first and second pulse strengths was 30 in the Sukharev study and only 2.5 in the model. If the model uses an appropriately strong first pulse, then the number of pores is very large and V_m during the second pulse drops so low that the pores cannot expand and no uptake takes place. To trigger pore expansion, the second pulse should exceed threshold, which would defeat the purpose of the two-pulse protocol. Thus, we have chosen to use a smaller first pulse, which limits the degree of electroporation and prevents a large drop in V_m. Of course, this adjustment would not have been necessary had the model represented a true cell, which would maintain a decent V_m even after a strong pulse.

Fortunately, our model of electroporation (Eqs. 1 and 3) can be used with spatially extended systems. For a single cell in an external field, the cell membrane can be divided into equipotential slices and Eqs. 1 and 3 will apply to each slice. All slices will be coupled by common membrane tension σ_{eff} and by V_m, which in a spatially extended system will be governed by a partial differential equation (PDE) instead of an ODE (Eq. 7). Such a model will be computationally more expensive, mostly because of the need to solve a PDE at each time step. Nevertheless, this approach has been used successfully in our previous studies that explored electroporation in a cell, a one-dimensional fiber, and a two-dimensional sheet of tissue, although with a much simpler electroporation model (Aguel et al., 1999; DeBruin and Krassowska, 1998, 1999).

In deriving Eq. 5 for effective membrane tension, the tension was assumed to depend linearly on the change in membrane area. This assumption breaks down in the low-tension regime, in which thermal fluctuations affect the shape of the membrane (Rawicz et al., 2000). The nonlinear area-tension relation may influence of the later stages of pore evolution. Another simplification is that the cell volume is assumed constant. In reality, the intracellular fluid will leak out through the macropores, resulting in reduced membrane tension. The reduced membrane tension will halt the tendency of pores to expand and will contribute to the eventual resealing of pores. Thus, another extension of this model should be the addition of changes in cell volume. The coupling of pore evolution with a change in cell volume has been proposed before, although for the case of only one pore present (Brochard-Wyart et al., 2000; Sandre et al., 1999).

The model of DNA permeation is the least developed part of this work. As a first step, we used the simplest available formulation proposed by Neumann et al. (1996), which is based on the Nernst-Planck equation. It is not clear to what extent this equation applies to long DNA chains (Puc et al., 2003). For example, it accounts for the DNA size only indirectly, through its effective charge z_{eff}. Also, the relative radii of the DNA and the pores affect permeation in a very simplistic way: a critical pore size is chosen (e.g., 10 nm) and pores below this size do not admit DNA. Clearly, there is room for improvement here. In the future, we plan to incorporate a more sophisticated model of DNA uptake, which will be based on the recent theoretical and experimental results related to the translocation of the DNA chain through the pore (Ambjörnsson et al., 2002; de Gennes, 1999; Han et al., 1999; Kasianowicz et al., 1996; Sung and Park, 1996).

An additional source of discrepancy between the model's predictions and experimental results is that the model is deterministic, whereas experiments contain numerous random components: cells differ in diameter and shape, which exposes them to different V_m in the same electric field, and the processes of pore creation, evolution, and DNA uptake are stochastic in nature (Powell and Weaver, 1986; Sung and Park, 1996). Were these random elements included in the model, as was done by Puc et al. (2003), certain results of this study would be modified. For example, the sharp drop in the DNA uptake for V_0 above 1.4 V is clearly unphysiological and results from the lack of random factors in the model.

Finally, this study could not even attempt to reproduce quantitatively the results of any particular experiment. The reason is twofold. First, the results reported in experiments, such as transfection efficiency (TE), cannot be related in a rigorous way to the intracellular DNA concentration predicted by the model. One study reported that TE, assessed by the activity of β-galactosidase, depended linearly on the external DNA concentration (Klenchin et al., 1991), and thus, also on the internal DNA concentration. However, no such relation was found in another study (Rols et al., 1998a), which indicates that TE, when measured hours or days after the experiment using bulk colorimetric methods, depends on a number of biological factors (Chang et al., 1991; Rols et al., 1998b; Sukharev et al., 1994). Second, it is not possible to find in the literature all parameters required by the model for a single cell type. The most comprehensive parameter set is available for artificial lipid bilayers, but experiments on lipid bilayers do not yield data on DNA uptake. On the other hand, cell lines used in the DNA uptake experiments have not been used in experiments that determine basic parameters of electroporation. Typically, only electroporation threshold is measured (Sukharev et al., 1992; Wolf et al., 1994), and sometimes the resealing time constant as well (Bier et al., 1999; Golzio et al., 1998; Hama-Inaba et al., 1987).

Relevance for electroporation-mediated DNA delivery

Even with these limitations, the predictions of the model are in qualitative and sometimes even quantitative agreement with experiments. Most important, the model confirms numerous experimental findings that pulses of millisecond

duration, slightly above the threshold for electroporation, are most effective in delivering DNA to cells, whereas the short and strong pulses used in drug delivery are not effective (Gehl and Mir, 1999; Hama-Inaba et al., 1987; Rols et al., 1998a; Yoshizato et al., 2000). The model explains these results by demonstrating that just suprathreshold pulses create pores large enough to admit DNA and of sufficient number to assure the postshock shrinkage of all pores to r_m, which facilitates resealing and cell survival (Tables 2 and 3). Larger pulses ($>$1.35 V) create many pores but they are too small for significant DNA uptake because they accumulate at a radius $<$10 nm (Tables 2 and 3). Thus, the predicted voltage range for successful uptake is relatively narrow (Fig. 6), which is consistent with some experimental results (e.g., ~1.2–1.6 kV/cm in Tekle et al., 1991). However, other studies observed a somewhat wider voltage range (e.g., maximum uptake observed at 2.5 times threshold in Hama-Inaba et al., 1987).

Two other key experimental findings are that the observable uptake of macromolecules requires a pulse duration on the order of milliseconds (Klenchin et al., 1991; Rols and Teissié, 1998) and that, for multipulse protocols, the uptake decreases with the break between pulses (Satkauskas et al., 2002; Sukharev et al., 1992; Wolf et al., 1994). These results are consistent with Table 3 and Fig. 7 *B*. The time constant of the decrease in uptake appears to be longer in experiments than in the model (e.g., minutes rather than seconds (Bier et al., 1999; Golzio et al., 1998; Satkauskas et al., 2002; Tekle et al., 1991)). This is because the resealing time constant in the model, ~3 s, comes from the measurements on the lipid bilayers (Glaser et al., 1988) and may not be appropriate for cell lines used experimentally.

The model can also explain the experimental observation that the permeable state is long-lived for small, but not large, molecules (Rols and Teissié, 1998; Satkauskas et al., 2002; Wolf et al., 1994). As seen in Fig. 5, in less than a millisecond after the pulse pores shrink to the minimum energy radius $r_m \approx 0.8$ nm, where they persist until resealing takes place. This radius is large enough to admit small marker molecules such as propidium iodide or calcein (radius $\approx$ 0.6 nm, evaluated from molecular weight (Fournier, 1998)), which can enter driven by the concentration gradient, but not for the macromolecules with a radius much larger than r_m.

It is not clear whether the model's prediction of the drop in the DNA uptake at very strong pulses (Table 2) agrees with experiments. The difficulty here is the decrease in the cell viability with the pulse strength, which may affect the measurement of the uptake. Some studies demonstrated a decrease in DNA uptake for strong pulses in several cell lines, but this decrease disappeared when the uptake per viable cell was reported (Chang et al., 1991; Hama-Inaba et al., 1987). On the other hand, other groups report a decrease in DNA uptake for strong pulses even if the cell viability decrease is taken into account (Tekle et al., 1991; Wolf et al., 1994).

Most important, our model greatly simplifies the intuitive picture of the DNA uptake by the cells, which is still debated in the literature. To date, theoretical models could predict stable pores of only a few nanometers in radius; larger pores were unstable (Freeman et al., 1994; Joshi and Schoenbach, 2000). These predictions were confirmed by some experiments, in which high-voltage, short pulses were used that must have created a large number of pores with radii not substantially larger than 1 nm (Glaser et al., 1988; Kakorin and Neumann, 2002; Schwister and Deuticke, 1985). To reconcile these results with the experimental evidence of the significant increase in DNA uptake after electric pulses, some researchers postulated that DNA entry into cells relies on the DNA-membrane interactions, which may be facilitated by a collection of small, 1 nm pores (Neumann et al., 1996; Rols and Teissié, 1998; Rols et al., 1998b; Sukharev et al., 1992, 1994). However, the physical mechanism behind such a permeation process remains unclear and direct experimental confirmation is still lacking.

Our model, together with the experimental and theoretical evidence of the existence of stable pores with radii on the order of tens to hundreds of nanometers (Chang and Reese, 1990; Fošnarič et al., 2003; Kandušer et al., 2003; Lieber and Steck, 1982; Sandre et al., 1999; Tieleman et al., 2003; Zhelev and Needham, 1993), supports a simpler mechanism, in which DNA enters the membrane through stable macropores. Our model predicts pores large enough to permit the uptake of DNA (Fig. 4; Tables 2 and 3), even in its circular or supercoiled conformation (Blackburn and Gait, 1996). These pores remain open for the entire duration of the electric pulse (Fig. 4; Tables 2 and 3) providing adequate time for the DNA chain to enter the cell (Rols and Teissié, 1998; Sukharev et al., 1994). Although this mechanism needs further experimental confirmation, the qualitative agreement between the modeling and experimental results, presented here, speaks in its favor. With further improvements, the model presented here may become a valuable tool in theoretical investigations of electroporation-mediated DNA delivery.

The authors thank Drs. S. B. Dev, D. P. Rabussay, N. B. Dev, and L. Zhang for their insightful comments and advice.

This work was supported in part by National Science Foundation grant BES-0108408.

REFERENCES

Abidor, I. G., V. B. Arakelyan, L. V. Chernomordik, Y. A. Chizmadzhev, V. F. Pastushenko, and M. R. Tarasevich. 1979. Electric breakdown of bilayer lipid membranes. I. Main experimental facts and their qualitative discussion. *Bioelectrochem. Bioenerg.* 6:37–52.

Aguel, F., K. A. DeBruin, W. Krassowska, and N. Trayanova. 1999. Effects of electroporation on the transmembrane potential distribution in a two-dimensional bidomain model of cardiac tissue. *J. Cardiovasc. Electrophysiol.* 10:701–714.

Aihara, H., and J. Miyazaki. 1998. Gene transfer into muscle by electroporation in vivo. *Nat. Biotechnol.* 16:867–870.

Ambjörnsson, T., S. P. Apell, Z. Konkoli, E. A. Di Marzio, and J. J. Kasianowicz. 2002. Charged polymer membrane translocation. *J. Chem. Phys.* 117:4063–4073.

Barnett, A., and J. C. Weaver. 1991. Electroporation: a unified, quantitative theory of reversible electrical breakdown and mechanical rupture in artificial planar bilayer membranes. *Bioelectrochem. Bioenerg.* 25: 163–182.

Benz, R., F. Beckers, and U. Zimmermann. 1979. Reversible electrical breakdown of lipid bilayer membranes: A charge-pulse relaxation study. *J. Membr. Biol.* 48:181–204.

Benz, R., and U. Zimmermann. 1980. Relaxation studies on cell membranes and lipid bilayers in the high electric field range. *Bioelectrochem. Bioenerg.* 7:723–739.

Bier, M., S. M. Hammer, D. J. Canaday, and R. C. Lee. 1999. Kinetics of resealing for transient electropores in isolated mammalian skeletal muscle cells. *Bioelectromagnetics.* 20:194–201.

Blackburn, G. M., and M. J. Gait. 1996. Nucleic Acids in Chemistry and Biology. Oxford University Press, Oxford, UK.

Brochard-Wyart, F., P. G. de Gennes, and O. Sandre. 2000. Transient pores in stretched vesicles: role of leak-out. *Physica A.* 278:32–51.

Chang, D. C., and T. S. Reese. 1990. Changes in membrane structure induced by electroporation as revealed by rapid-freezing electron microscopy. *Biophys. J.* 58:1–12.

Chang, D. C., P.-Q. Gao, and B. L. Maxwell. 1991. High efficiency gene transfection using a radio-frequency electric field. *Biochim. Biophys. Acta.* 1992:153–160.

Chernomordik, L. V., S. I. Sukharev, I. G. Abidor, and Y. A. Chizmadzhev. 1983. Breakdown of lipid bilayer membranes in an electric field. *Biochim. Biophys. Acta.* 736:203–213.

Chernomordik, L. V., S. I. Sukharev, S. V. Popov, V. F. Pastushenko, A. V. Sokirko, I. G. Abidor, and Y. A. Chizmadzhev. 1987. The electrical breakdown of cells and lipid membranes: the similarity of phenomenologies. *Biochim. Biophys. Acta.* 902:360–373.

DeBruin, K. A., and W. Krassowska. 1998. Electroporation and shock-induced transmembrane potential in a cardiac fiber during defibrillation strength shocks. *Ann. Biomed. Eng.* 26:584–596.

DeBruin, K. A., and W. Krassowska. 1999. Modeling electroporation in a single cell. I. Effects of field strength and rest potential. *Biophys. J.* 77:1213–1224.

de Gennes, P. G. 1999. Passive entry of a DNA molecule into a small pore. *Proc. Natl. Acad. Sci. USA.* 96:7262–7264.

Dev, S. B., D. P. Rabussay, G. Widera, and G. A. Hofmann. 2000. Medical applications of electroporation. *IEEE Trans. Plasma Sci.* 28:206–223.

Fournier, R. L. 1998. Basic Transport Phenomena in Biomedical Engineering. Taylor & Francis, Philadelphia, PA.

Fošnarič, M., V. Kralj-Iglič, K. Bohinc, A. Iglič, and S. May. 2003. Stabilization of pores in lipid bilayers by anisotropic inclusions. *J. Phys. Chem. B.* 107:12519–12526.

Freeman, S. A., M. A. Wang, and J. C. Weaver. 1994. Theory of electroporation of planar bilayer membranes: predictions of the aqueous area, change in capacitance, and pore-pore separation. *Biophys. J.* 67: 42–56.

Gabriel, B., and J. Teissié. 1997. Direct observation in the millisecond time range of fluorescent molecule asymmetrical interaction with the electropermeabilized cell membrane. *Biophys. J.* 73:2630–2637.

Gehl, J., and L. M. Mir. 1999. Determination of optimal parameters for in vivo gene transfer by electroporation, using a rapid in vivo test for cell permeabilization. *Biochem. Biophys. Res. Commun.* 261:377–380.

Glaser, R. W. 1986. Appearance of a ''critical voltage'' in reversible electric breakdown. *Stud. Biophys.* 16:77–86.

Glaser, R. W., S. L. Leikin, L. V. Chernomordik, V. F. Pastushenko, and A. I. Sokirko. 1988. Reversible electrical breakdown of lipid bilayers: formation and evolution of pores. *Biochim. Biophys. Acta.* 940:275–287.

Golzio, M., M.-P. Mora, C. Raynaud, C. Delteil, J. Teissié, and M.-P. Rols. 1998. Control by osmotic pressure of voltage-induced permeabilization and gene transfer in mammalian cells. *Biophys. J.* 74:3015–3022.

Gowrishankar, T. R., and J. C. Weaver. 2003. An approach to electrical modeling of single and multiple cells. *Proc. Natl. Acad. Sci. USA.* 100:3203–3208.

Hama-Inaba, H., M. Takahashi, M. Kasai, T. Shiomi, A. Ito, F. Hanaoka, and K. Sato. 1987. Optimum conditions for electric pulse mediated gene transfer to mammalian cells in suspension. *Cell Struct. Funct.* 12: 173–180.

Han, J., S. W. Turner, and H. G. Craighead. 1999. Entropic trapping and escape of long DNA molecules at submicron size constriction. *Phys. Rev. Lett.* 83:1688–1691.

Hibino, M., M. Shigemori, H. Itoh, K. Nagayama, and K. Kinosita Jr. 1991. Membrane conductance of an electroporated cell analyzed by submicrosecond imaging of transmembrane potential. *Biophys. J.* 59:209–220.

Israelachvili, J. 1992. Intermolecular and Surface Forces, 2nd ed. Academic Press, London, UK.

Joshi, R. P., and K. H. Schoenbach. 2000. Electroporation dynamics in biological cells subjected to ultrafast electrical pulses: a numerical simulation study. *Phys. Rev. E.* 62:1025–1033.

Joshi, R. P., Q. Hu, K. H. Schoenbach, and H. P. Hjalmarson. 2002. Improved energy model for membrane electroporation in biological cells subjected to electrical pulses. *Phys. Rev. E.* 65:041920-1–041920-8.

Kakorin, S., and E. Neumann. 2002. Ionic conductivity of electroporated lipid bilayer membranes. *Bioelectrochemistry.* 56:163–166.

Kandušer, M., M. Fošnarič,, M. Šentjurc, V. Kralj-Iglič, H. Hägerstrand, A. Iglič, and D. Miklavčič. 2003. Effect of surfactant polyoxyethylene glycol (C12E8) on electroporation of cell line DC3F. *Colloid. Surface. A.* 214:205–217.

Kasianowicz, J. J., E. Brandin, D. Branton, and D. W. Deamer. 1996. Characterization of individual polynucleotide molecules using a membrane channel. *Proc. Natl. Acad. Sci. USA.* 93:13770–13773.

Klenchin, V. A., S. I. Sukharev, S. M. Serov, L. V. Chernomordik, and Y. A. Chizmadzhev. 1991. Electrically induced DNA uptake by cells is a fast process involving DNA electrophoresis. *Biophys. J.* 60:804–811.

Lieber, M. R., and T. L. Steck. 1982. A description of the holes in human erythrocyte membrane ghosts. *J. Biol. Chem.* 257:11651–11659.

Matthews, K. E., S. B. Dev, F. Toneguzzo, and A. Keating. 1995. Electroporation for gene therapy. *In* Methods in Molecular Biology, Vol. 48: Animal Cell Electroporation and Electrofusion Protocols. J. A. Nickoloff, editor. Humana Press, Totowa, NJ. 273–280.

McNeil, P. L., and R. A. Steinhardt. 1997. Loss, restoration and maintenance of plasma membrane integrity. *J. Cell Biol.* 137:1–4.

Neu, J. C., and W. Krassowska. 1999. Asymptotic model of electroporation. *Phys. Rev. E.* 59:3471–3482.

Neu, J. C., and W. Krassowska. 2003. Modeling postshock evolution of large electropores. *Phys. Rev. E.* 67:021915-1–021915-12.

Neu, J. C., K. C. Smith, and W. Krassowska. 2003. Electrical energy required to form large conducting pores. *Bioelectrochem. Bioenerg.* 60:107–114.

Neumann, E., S. Kakorin, I. Tsoneva, B. Nikolova, and T. Tomov. 1996. Calcium-mediated DNA adsorption to yeast cells and kinetics of cell transformation by electroporation. *Biophys. J.* 71:868–877.

Newman, J. 1966. Resistance for flow of current to a disk. *J. Electrochem. Soc.* 113:501–502.

Nishi, T., K. Yoshizato, H. Takeshima, K. Sato, K. Hamada, I. Kitamura, T. Yoshimura, H. Saya, J. Kuratsu, and Y. Ushio. 1996. High-efficiency in vivo gene transfer using intraarterial plasmid DNA injection following in vivo electroporation. *Cancer Res.* 56:1050–1055.

Pastushenko, V. F., and Y. A. Chizmadzhev. 1982. Stabilization of conducting pores in BLM by electric current. *Gen. Physiol. Biophys.* 1:43–52.

Pavlin, M., and D. Miklavčič. 2003. Effective conductivity of a suspension of permeabilized cells: a theoretical analysis. *Biophys. J.* 85:719–729.

Plonsey, R., and R. C. Barr. 1988. Bioelectricity. A Quantitative Approach. Plenum Press, New York, NY.

Potter, H. 1988. Electroporation in biology: methods, applications, and instrumentation. *Anal. Biochem.* 174:361–373.

Powell, K. T., A. W. Morgenthaler, and J. C. Weaver. 1989. Tissue electroporation. Observation of reversible electrical breakdown in viable frog skin. *Biophys. J.* 56:1163–1171.

Powell, K. T., and J. C. Weaver. 1986. Transient aqueous pores in bilayer membranes: a statistical theory. *Bioelectrochem. Bioenerg.* 15:211–227.

Puc, M., T. Kotnik, L. M. Mir, and D. Miklavčič. 2003. Quantitative model of small molecules uptake after in vitro cell electropermeabilization. *Bioelectrochemistry.* 60:1–10.

Rawicz, W., K. C. Olbrich, T. McIntosh, D. Needham, and E. Evans. 2000. Effect of chain length and unsaturation on elasticity of lipid bilayers. *Biophys. J.* 79:328–339.

Rols, M.-P., C. Delteil, M. Golzio, P. Dumond, S. Cros, and J. Teissié. 1998a. In vivo electrically mediated protein and gene transfer in murine melanoma. *Nat. Biotechnol.* 16:168–171.

Rols, M.-P., C. Delteil, and J. Teissié. 1998b. Control by ATP and ADP of voltage-induced mammalian-cell-membrane permeabilization, gene transfer and resulting expression. *Eur. J. Biochem.* 254:382–388.

Rols, M.-P., and J. Teissié. 1998. Electropermeabilization of mammalian cells to macromolecules: control by pulse duration. *Biophys. J.* 74:1415–1423.

Rybenkov, V. V., A. V. Vologodskii, and N. R. Cozzarelli. 1997. The effect of ionic conditions on the conformations of supercoiled DNA. I. Sedimentation analysis. *J. Mol. Biol.* 267:299–311.

Sandre, O., L. Moreaux, and F. Brochard-Wyart. 1999. Dynamics of transient pores in stretched vesicles. *Proc. Natl. Acad. Sci. USA.* 96:10591–10596.

Satkauskas, S., M. F. Bureau, M. Puc, A. Mahfoudi, D. Scherman, D. Miklavčič, and L. M. Mir. 2002. Mechanisms of in vivo DNA electrotransfer: respective contributions of cell electropermeabilization and DNA electrophoresis. *Mol. Ther.* 5:133–140.

Schwister, K., and B. Deuticke. 1985. Formation and properties of aqueous leaks induced in human erythrocytes by electrical breakdown. *Biochim. Biophys. Acta.* 816:332–348.

Sukharev, S. I., V. A. Klenchin, S. M. Serov, L. V. Chernomordik, and Y. A. Chizmadzhev. 1992. Electroporation and electrophoretic DNA transfer into cells. The effect of DNA interaction with electropores. *Biophys. J.* 63:1320–1327.

Sukharev, S. I., A. V. Titomirov, and V. A. Klenchin. 1994. Electrically induced DNA transfer into cells. Electroporation in vivo. *In* Gene Therapeutics: Methods and Applications of Direct Gene Transfer. J. A. Wolff, editor. Birkhäuser, Boston, MA. 210–232.

Sung, W., and P. J. Park. 1996. Polymer translocation through a pore in a membrane. *Phys. Rev. Lett.* 77:783–786.

Tekle, E., R. D. Astumian, and P. B. Chock. 1991. Electroporation by using bipolar oscillating electric field: an improved method for DNA transfection of NIH 3T3 cells. *Proc. Natl. Acad. Sci. USA.* 88:4230–4234.

Tieleman, D. P., H. Leontiadou, A. E. Mark, and S.-J. Marrink. 2003. Simulation of pore formation in lipid bilayers by mechanical stress and electric fields. *J. Am. Chem. Soc.* 125:6382–6383.

Weaver, J. C. 1994. Molecular basis for cell membrane electroporation. *Ann. N. Y. Acad. Sci.* 720:141–152.

Weaver, J. C., and Y. A. Chizmadzhev. 1996. Theory of electroporation: a review. *Bioelectrochem. Bioenerg.* 41:135–160.

Weidmann, S. 1970. Electrical constants of trabecular muscle from mammalian heart. *J. Physiol.* 210:1041–1054.

Wolf, H., M.-P. Rols, E. Boldt, E. Neumann, and J. Teissié. 1994. Control by pulse parameters of electric field–mediated gene transfer in mammalian cells. *Biophys. J.* 66:524–531.

Xie, T. D., and T. Y. Tsong. 1992. Study of mechanisms of electric field-induced DNA transfection. III. Electric parameters and other conditions for effective transfection. *Biophys. J.* 63:28–34.

Yoshizato, K., T. Nishi, T. Goto, S. B. Dev, H. Takeshima, T. Kino, K. Tada, T. Kimura, S. Shiraishi, M. Kochi, J.-I. Kuratsu, G. A. Hofmann, and Y. Ushio. 2000. Gene delivery with optimized electroporation parameters shows potential for treatment of gliomas. *Int. J. Oncol.* 16:899–905.

Zewert, T. E., U. F. Pliquett, R. Langer, and J. C. Weaver. 1995. Transdermal transport of DNA antisense oligonucleotides by electroporation. *Biochem. Biophys. Res. Commun.* 212:286–292.

Zhang, L., L. Li, G. A. Hofmann, and R. M. Hoffman. 1996. Depth-targeted efficient gene delivery and expression in the skin by pulsed electric fields: an approach to gene therapy of skin aging and other diseases. *Biochem. Biophys. Res. Commun.* 220:633–636.

Zhelev, D. V., and D. Needham. 1993. Tension-stabilized pores in giant vesicles: determination of pore size and pore line tension. *Biochim. Biophys. Acta.* 1147:89–104.